
Flow, Turbulence and Combustion **66:** 159–182, 2001.

Experiments in Turbulent Pipe Flow with Polymer Additives at Maximum Drag Reduction

P.K. PTASINSKI, F.T.M. NIEUWSTADT, B.H.A.A. VAN DEN BRULE and M.A. HULSEN
J.M. Burgers Centre for Fluid Dynamics, Delft University of Technology, Leeghwaterstraat 21, 2628 CA Delft, The Netherlands

Received 8 February 2000; accepted in revised form 10 April 2001

Abstract. In this paper we report on (two-component) LDV experiments in a fully developed turbulent pipe flow with a drag-reducing polymer (partially hydrolyzed polyacrylamide) dissolved in water. The Reynolds number based on the mean velocity, the pipe diameter and the local viscosity at the wall is approximately 10000. We have used polymer solutions with three different concentrations which have been chosen such that maximum drag reduction occurs. The amount of drag reduction found is 60–70%. Our experimental results are compared with results obtained with water and with a very dilute solution which exhibits only a small amount of drag reduction.

We have focused on the observation of turbulence statistics (mean velocities and turbulence intensities) and on the various contributions to the total shear stress. The latter consists of a turbulent, a solvent (viscous) and a polymeric part. The polymers are found to contribute significantly to the total stress. With respect to the mean velocity profile we find a thickening of the buffer layer and an increase in the slope of the logarithmic profile. With respect to the turbulence statistics we find for the streamwise velocity fluctuations an increase of the root mean square at low polymer concentration but a return to values comparable to those for water at higher concentrations. The root mean square of the normal velocity fluctuations shows a strong decrease. Also the Reynolds (turbulent) shear stress and the correlation coefficient between the streamwise and the normal components are drastically reduced over the entire pipe diameter. In all cases the Reynolds stress stays definitely non-zero at maximum drag reduction. The consequence of the drop of the Reynolds stress is a large polymer stress, which can be 60% of the total stress. The kinetic-energy balance of the mean flow shows a large transfer of energy directly to the polymers instead of the route by turbulence. The kinetic energy of the turbulence suggests a possibly negative polymeric dissipation of turbulent energy.

Key words: maximum drag reduction, polymer additives, turbulent pipe flow.

1. Introduction

Dissolving a small amount of polymers (usually a few weight parts per million) in water can drastically reduce the pressure drop (or frictional drag) of turbulent pipe or channel flow. This phenomenon was first discovered by Toms [1] and has received a lot of attention afterwards because of its practical use in various applications such as for instance oil pipe lines and sewer systems. Though the polymers are primarily active on the smallest length scales, they are able to influence the macroscopic scales of the flow by which the drag is determined. Therefore, un-

derstanding the phenomenon of drag reduction is challenging from a fundamental point of view.

The additives causing drag reduction can be divided in three groups: polymers, surfactants and fibres. A detailed description of the drag reduction phenomenon is given by Gyr and Bewersdorff [2]. In this paper we will restrict ourselves to drag reduction of turbulent pipe flow by long flexible polymers, which are dissolved in water.

Over the past decades numerous studies have been carried out on drag reduction by polymer additives. For a review of the early work on this subject we refer to Lumley [3] who outlines the different physical phenomena of drag reduction and to Virk [4] who presents experimental evidence that drag reduction is limited by an asymptotic value. Furthermore, the book of Gyr and Bewersdorff [2] gives an extensive overview of the more recent material on the subject. A few studies deserve to be mentioned separately. Lumley [5] describes the changes of turbulent structures postulates that stretching of randomly coiled polymers due to strong turbulent flow is relevant for drag reduction. The changes of turbulent structures in the buffer layer are also discussed by Tiederman [6]. Den Toonder et al. [7] have shown that simulations with a model having viscous anisotropic stresses give results that are consistent with experimental observations. Sureshkumar et al. [8] present results of direct numerical simulations of a dilute polymer solution where polymer chains are modelled as FENE-P dumbbells.

With respect to experiments on turbulent flow with polymer additives we can mention the studies of Harder and Tiederman [9], Wei and Willmarth [10] and Willmarth et al. [11] who have made observations in a channel flow. Den Toonder et al. [7] and Den Toonder [12] have carried out experiments in a pipe flow. All experiments mentioned above have been performed with very low polymer concentrations, leading to a small amount of drag reduction. Observations in channel flow at higher rates of drag reduction are performed by Gampert and Yong [13], who discuss the influence on velocity statistics and coherent structures. Warholic et al. [14, 15] present experiments with surfactant and with polymer solutions. These two studies suggest that the Reynolds shear stress becomes negligible near maximum drag reduction.

The result of Warholic et al. [14, 15] that the Reynolds stress is close to zero has large implications for the turbulence and its production in polymeric flows. Therefore, in the present study we perform experiments of turbulent pipe flow with polymer additives at maximal drag reduction. These conditions are close to the maximum drag reduction (MDR) asymptote, also known as the Virk [4] asymptote. To interpret the effects of the polymers on turbulence at these high concentrations, we will compare the results to data for Newtonian flow (water) and to results obtained with very dilute solutions [7, 12]. Our objective is to investigate the effect of polymer additives on various elements of the flow statistics like turbulence intensities and stresses. Furthermore, we will focus our attention on the role of the polymer stresses and the various contributions to the total shear stress. We are able

to integrate kinetic energy budget terms over the entire pipe section and discuss these contributions in the energy balance.

The outline of this paper is as follows: in Section 2 we describe the main features of turbulent drag reducing flows and introduce the definitions of the parameters that we aim to measure. The experimental setup together with the LDV is discussed in Section 3. In Section 4 we will present the results of the LDV experiments mainly focusing on the polymer stresses and energy budget terms. Finally the main conclusions will be drawn in Section 5.

2. Turbulent Pipe Flow Characteristics

2.1. Mean flow

We consider a fully developed turbulent flow through a straight pipe with diameter D. The mean shear stress at the wall, τ_w, for Newtonian and non-Newtonian fluids and for all flow regimes is given by

$$\tau_w = \frac{D}{4}\frac{\Delta P}{\Delta x}, \tag{1}$$

where $\Delta P/\Delta x$ is the constant pressure gradient. The wall shear stress is usually expressed in terms of the Fanning friction factor f given by

$$f = \frac{\tau_w}{\frac{1}{2}\rho {U_b}^2} \tag{2}$$

with U_b the mean velocity in the pipe and ρ the density of the fluid. For instance, the expressions for f for laminar and fully turbulent pipe flow of a Newtonian fluid are, respectively (see [16]):

$$f = \frac{16}{\mathrm{Re}}, \tag{3}$$

$$f^{-1/2} = 4.0\log(\mathrm{Re}\, f^{1/2}) - 0.4, \tag{4}$$

$\mathrm{Re} = \rho U_b D/\eta$ is the Reynolds number based on the constant viscosity η of the fluid.

For polymeric liquids the viscosity is in general shear-rate dependent, so that the usual definition of the Reynolds number cannot be used. In this paper we use a method proposed by Pinho and Whitelaw [17] and Draad et al. [18]. In this approach the Reynolds number is based on the viscosity at the pipe wall (η_w) as obtained from

$$\eta_w = \frac{\tau_w}{\dot{\gamma}_w}, \tag{5}$$

where $\eta_w \equiv \eta(\dot{\gamma}_w)$ and $\dot{\gamma}_w$ is the local shear rate at the wall.

The relation between the viscosity and the shear rate follows from observations in a viscometer. In our case we have used a low shear viscometer (Contraves LS-40) with a Couette geometry. To the observations we have fitted the Carreau model [19] given by

$$\eta(\dot{\gamma}) = \eta_\infty + (\eta_0 - \eta_\infty)\left[1 + (\lambda\dot{\gamma})^2\right]^{(n-1)/2}, \tag{6}$$

in which η_0 is the zero-shear-rate viscosity, η_∞ is the infinite-shear-rate viscosity, λ is a time constant and n is the dimensionless power law index. For the infinite-shear-rate viscosity the viscosity of the solvent (water) is taken. For a given value of τ_w (which is known from pressure drop measurements) the corresponding η_w and $\dot{\gamma}_w$ can then be determined by solving Equations (5) and (6) numerically. The wall Reynolds number is then defined by $\mathrm{Re}_w = \rho U_b D/\eta_w$.

As a check on this approach we have determined the shear rate at the wall as the derivative of the streamwise velocity (U_x, measured with LDV) with $\dot{\gamma}_w = -\mathrm{d}U_x/\mathrm{d}r$ for $r = D/2$. It turns out that the two values of $\dot{\gamma}_w$ (the numerical procedure with the Carreau model and LDV) are within 3% so that our procedure appears to be well justified.

At maximum drag reduction of non-shear-thinning fluids the friction law approaches an empirical asymptote, called the Virk [4] or maximum drag reduction asymptote given by

$$f^{-1/2} = 19.0\log(\mathrm{Re}\, f^{1/2}) - 32.4. \tag{7}$$

For shear-thinning fluids Gyr and Bewersdorff [2, p. 105] show that plotting of the friction factor vs. the wall Reynolds number collapses the data near Virk asymptote. This does not happen when we use the Reynolds number based on the viscosity of water. Therefore we will use the wall Reynolds number Re_w in Equation (7).

The amount of (percentual) drag reduction is defined as the percentual reduction of pressure-drop due to the addition of the polymers:

$$\mathrm{DR}\% = \frac{\Delta P_\mathrm{N} - \Delta P_\mathrm{P}}{\Delta P_\mathrm{N}} \cdot 100\% = \frac{f_\mathrm{N} - f_\mathrm{P}}{f_\mathrm{N}} \cdot 100\% \tag{8}$$

at the same wall Reynolds number. The suffices 'N' and 'P' stand for the Newtonian (non-drag-reducing) and the polymeric (drag-reducing) fluid respectively.

2.2. Description of turbulent pipe flow

2.2.1. *Basic Equations*

We use a cylindrical coordinate system (x, r, θ) for the axial, radial and tangential coordinate respectively. For the basic equations of motion formulated in this coordinate system we refer to a standard text such as Batchelor [20]. The total stress is decomposed in a solvent part (Newtonian) and a polymeric part (non-Newtonian) according to:

$$\tau_{ij} = \tau_{s,ij} + \tau_{p,ij} = 2\eta_s e_{ij} + \tau_{p,ij}, \tag{9}$$

where η_s is the solvent (water) viscosity and e_{ij} the rate-of-deformation tensor. The well-known Reynolds decomposition is used for the velocity vector $u_i = (u_x, u_r, u_\theta)$, the pressure p and the polymeric stress $\tau_{p,ij}$, in which lower case with a prime denotes a fluctuation and upper case denotes a mean value (alternatively, a mean value is sometimes indicated by brackets $\langle \cdots \rangle$). For a stationary fully developed flow the equation for the mean axial momentum becomes

$$0 = -\frac{\partial P}{\partial x} + \frac{1}{r}\frac{\partial}{\partial r}\left\{ r\left(-\rho\langle u_x' u_r' \rangle + \eta_s \frac{\partial U_x}{\partial r} + \mathcal{T}_{p,rx} \right) \right\}. \tag{10}$$

2.2.2. *Kinetic Energy of the Mean Flow and of the Turbulence*

The equation for the mean flow kinetic energy, $(1/2)\rho U_i U_i$, can be written as:

$$\begin{aligned} 0 \;=\; & \underbrace{-U_x \frac{\partial P}{\partial x}}_{P_u} + \underbrace{\frac{1}{r}\frac{\partial}{\partial r}\left(r U_x \left(-\rho\langle u_x' u_r' \rangle + \eta_s \frac{\partial U_x}{\partial r} + \mathcal{T}_{p,rx} \right) \right)}_{T_u} \\ & + \underbrace{\rho\langle u_x' u_r' \rangle \frac{\partial U_x}{\partial r}}_{D_u} - \underbrace{\eta_s \left(\frac{\partial U_x}{\partial r} \right)^2}_{E_s} - \underbrace{\mathcal{T}_{p,rx} \frac{\partial U_x}{\partial r}}_{E_p}. \end{aligned} \tag{11}$$

This equation is integrated over the cross-section in order to obtain a balance over the entire section. P_u is the production of mean flow energy by the imposed pressure gradient. The three terms in T_u describe the transport of mean flow energy by respectively Reynolds stresses, mean viscous stresses and mean polymeric stresses. When integrated over the cross-section of the pipe and under the of assumption symmetry around the centreline, the contribution of T_u to the area-averaged energy budget is zero. D_u is called deformation work and becomes production in the equation for the turbulent kinetic energy, Equation (12). E_s is the viscous dissipation by the mean flow and E_p is the dissipation by mean polymeric stresses. In the area-averaged budget P_u is positive and the remaining terms (D_u, $-E_s$ and $-E_p$) are negative.

The equation for the kinetic energy of the turbulence, $(1/2)\rho\langle u_i' u_i' \rangle$, reads

$$\begin{aligned} 0 \;=\; & \underbrace{-\rho\langle u_x' u_r' \rangle \frac{\partial U_x}{\partial r}}_{P_k} \\ & + \underbrace{\frac{1}{r}\frac{\partial}{\partial r}\left(r\left(-\frac{1}{2}\rho\langle u_r' u_i' u_i' \rangle - \langle p' u_r' \rangle + \frac{1}{2}\eta_s \frac{\partial}{\partial r}\langle u_i' u_i' \rangle + \langle u_i' \tau_{p,ir}' \rangle \right) \right)}_{T_k} \\ & - \underbrace{\eta_s \left\langle \frac{\partial u_i'}{\partial x_j} \frac{\partial u_i'}{\partial x_j} \right\rangle}_{\epsilon_s} - \underbrace{\left\langle \tau_{p,ij}' \frac{\partial u_i'}{\partial x_j} \right\rangle}_{\epsilon_p} \end{aligned} \tag{12}$$

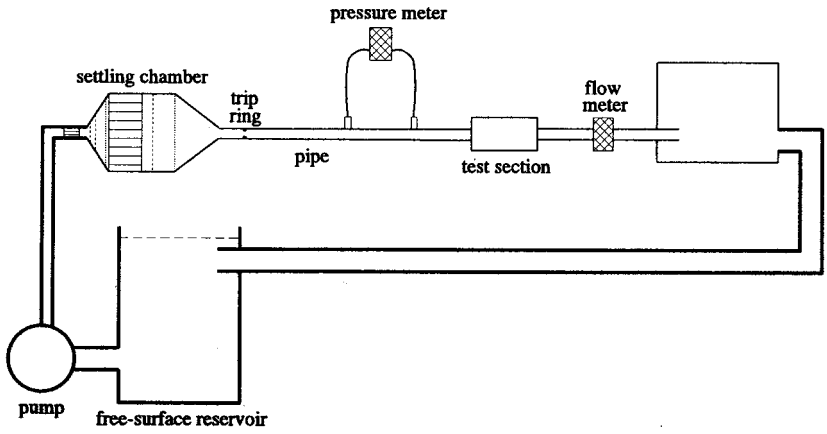

Figure 1. Schematic overview of the experimental facility.

Here, P_k is the production of turbulent kinetic energy. Since $P_k = -D_u$ we find that P_k is positive. The four terms in T_k result again in redistribution of turbulent kinetic energy and do not contribute to the balance when integrating over the pipe section. They represent the transport due to velocity fluctuations, due to pressure fluctuations, due to fluctuating viscous stresses and due to fluctuating polymeric stresses, respectively. The last two terms are the viscous (solvent) dissipation and the polymeric stress work. The viscous (solvent) dissipation is positive, whereas the sign of the polymeric stress work is unknown.

These budgets of the kinetic energy will be discussed further in Section 4.3.

3. Experimental Setup

3.1. Flow facility and measuring equipment

A detailed overview of the facility and the measuring equipment that we have used for our experiments, can be found in [12, 18, 21]. Here we will only mention the most important characteristics.

A schematic overview of the facility is shown in Figure 1. The main part of the setup consists of a smooth straight pipe with a length of 34 m and an inner diameter of 40.37 mm. The pipe has a circular cross-section and is made of transparent Plexiglas. The fluid is pumped from an open reservoir by a disc pump. This type of pump was selected because it minimizes the amount of mechanical degradation when working with polymer solutions (mechanical degradation of polymers will be discussed further in Section 3.2). After the pump the flow passes through a straightening device and a settling chamber. Just after the entrance of the pipe the flow is forced to turbulence by means of a (disturbance or trip) ring. At the exit of the pipe the flow returns through a discharge chamber and a return pipe to the reservoir. The volume of the whole facility under normal operating conditions is 1.5 m^3. The whole pipe is insulated in order to avoid temperature variations which

may cause secondary flow. LDV measurements show that secondary flows do not occur.

The velocity statistics are measured with a two-component LDV system in backscatter mode and in combination with two Burst Spectrum Analysers (BSA). The dimensions of the measurement volume are approximately 20, 20 and 100 μm in the streamwise (axial), normal (radial) and spanwise (tangential) direction, respectively. The data rate of the LDV signal used for the calculation of the flow statistics is approximately 30 Hz. The actual data rate is higher but in order to avoid velocity bias the measurements are performed in so-called dead time mode. This means that only one burst is accepted during the period of the dead time. The data presented in this paper are obtained with a measuring time of 240 s for each radial position. The estimated (relative) statistical errors are: approximately 2% for the first moment (mean velocity) and 4% for the second moment (root mean squares and stresses).

The use of LDV for a pipe flow as in our case, is complicated by the optical refraction due to the curved surface of the pipe. To minimize this problem, a small part of the pipe is replaced by a special test section. The test section consists of a rectangular Plexiglas box which is placed around the pipe. The pipe wall inside the optical box is replaced by a thin cylindrical sheet of Teflon FEP with a thickness of 190 μm. The refractive index of the sheet is $n = 1.344$ which is close to that of water ($n = 1.33$) so that refraction of the laser beams is minimized. The location of the test section is 26 m after the entrance of the pipe where the flow is fully developed.

The 2D-LDV probe is placed on a traversing mechanism operated by a PC. For our experiments we performed vertical traverses along the symmetry line of the test section while measuring the streamwise and normal velocity components simultaneously.

The flow rate through the pipe is measured with a magnetic inductive flow meter of Krohne-Altometer just after the test section. The accuracy of this flow meter is 0.4%. The temperature of the fluid is measured with two thermometers in the reservoir and in the discharge chamber. Measurements show that the temperature remains constant within 0.2 °C during a measurement of the velocity profile.

The pressure drop over a segment of the pipe is measured with a membrane differential pressure transducer (Validyne Engineering Corp.) with 88 mm water pressure full scale. The length of this segment is 8 m, which is chosen as large as possible in order to minimize the relative measuring error. The segment starts 16 m (400 pipe diameters) after the entrance of the pipe. The flow is fully developed as the pressure gradient is constant in the entire segment. Draad [21] has shown that for non-Newtonian flow this is the case after 280 pipe diameters.

3.2. POLYMER SOLUTIONS AND RHEOLOGICAL CHARACTERISATION

The polymer solutions used in these experiments consist of Superfloc A110 (Cytec Industries), which is a partially hydrolyzed polyacrylamide (PAMH). The molecular weight of this polymer which consists of approximately 10^5 monomers, is $6–8 \cdot 10^6$ g/mol. This polymer is dissolved in water following the procedure described below.

Due to the flow through the pipe and especially through the pump, the polymer solution is subject to very high rates of deformation which causes mechanical degradation. Mechanical degradation is the process of rupture of the polymers into smaller molecules or break-up of aggregates due to mechanical forces. The molecular weight is thus reduced which leads to a strong decrease of drag reduction. We have chosen Superfloc A110, because this molecule has been found to be better resistant to mechanical degradation [22] compared to other drag reducing polymers.

Mechanical degradation can be especially problematic for measurements which are to remain near maximum drag reduction. Therefore, we have added an excess of polymers to the flow in order to make sure that the flow conditions remain near this asymptote during the whole experiment. Inerthal and Wilski [23] and Kenis [24] state that such an excess of polymers leads to a decrease of the effects of degradation. In our measurements the pressure drop remains constant during an experiment. Furthermore we measured the shear viscosity of the fluids at the begin and at the end of an experiment and this does not change.

The solutions are prepared by first creating a solution with a fixed concentration (e.g. 3000 weight parts per million) of Superfloc A110 in water. This is done by slowly dissolving the polymers in water in a stirred vessel. After stirring for about 10 hours the mixture is left alone in order to let small air bubbles escape from the vessel. Finally this solution is diluted with fresh water until the prescribed concentration is obtained and pumped into the system. The solution is mixed slowly in the free surface reservoir and in the entire setup until it becomes homogeneous. Note that there is a difference between our experiments, where the polymer solution is first made homogeneous and then circulated during the experiments and the work of Warholic et al. [15] in which the polymer is injected. In the LDV measurements we have used solutions consisting of 103, 175 and 435 wppm (weight parts per million) Superfloc A110.

For these polymer solutions we have determined the viscosity as a function of shear rate. This is done at the same temperature at which the LDV measurements are carried out. The viscosity curves are fitted with the Carreau model as described by Equation (6) with $\eta_\infty = \eta_{\text{solvent}} = \eta_{\text{water}}$. In Table I the Carreau parameters for the three polymer solutions are given. The viscosity curves are presented in Figure 2.

Table I. Carreau parameters of the three polymer solutions used in the LDV experiments as defined in Equation (6).

solution	103 wppm	175 wppm	435 wppm
temp. (°C)	18.0	18.4	17.4
η_0 (mPas)	3.005	4.446	10.60
η_∞ (mPas)	1.053	1.043	1.090
n	0.7906	0.7605	0.7185
λ (s)	0.4359	0.4543	0.5635

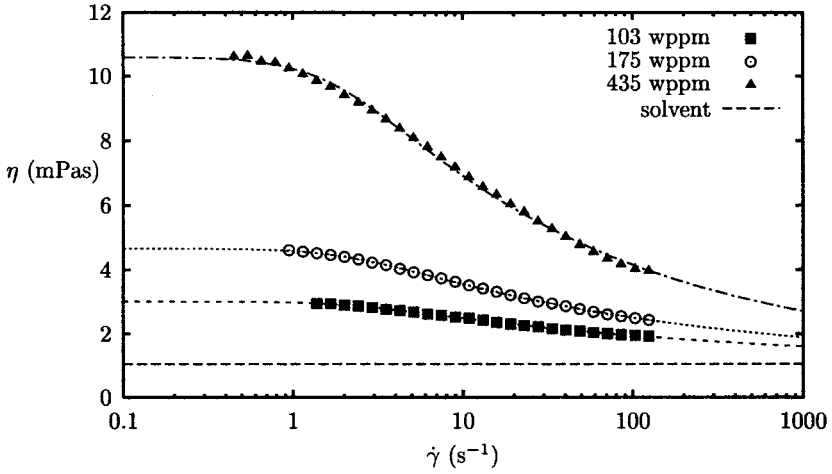

Figure 2. Viscosity as a function of shear rate for the three polymer solutions used in the LDV experiments. Symbols: measurement; lines: fit.

4. Experimental Results

4.1. Pressure drop measurements

For water, for the 103 and 435 wppm solutions we have carried out measurements of the Fanning friction factor for a range of (wall) Reynolds numbers. These results are shown in Figure 3. The corresponding LDV measurements (see Section 4.2) are also presented in this figure (denoted with '+').

We find that the 103 wppm solution shows slightly less drag reduction than Virk asymptote. The 175 wppm solution shows approximately the same drag reduction as the asymptote and the 435 wppm solution even exceeds it. This latter effect can be caused by the strong shear-thinning behaviour of the fluid, which might lead to inaccuracy in the determination of the wall viscosity and hence the wall Reynolds number.

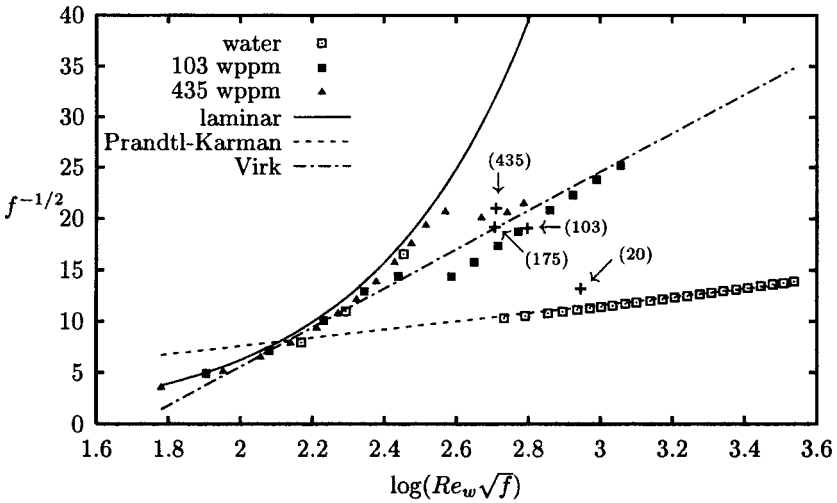

Figure 3. The relation between the friction factor and the (wall) Reynolds number in Prandtl–Karman coordinates. The LDV measurements which will be discussed in Section 4.2, are denoted with +, together with the concentration in wppm in brackets. The data of f for water and for the 103 and 435 wppm solutions are presented at a number of (wall) Reynolds numbers as indicated for the symbols. The three lines refer to Equations (3), (4), and (7).

Table II. Results of the friction factor measurements during the LDV experiments. Q: flow rate; Re_w: wall Reynolds number; $\dot{\gamma}_w$: local shear rate at the wall; τ_w: shear stress at the wall; f: friction factor determined with pressure drop measurement; DR%: percentual drag reduction as defined by Equation (8).

solution	water	20 wppm	103 wppm	175 wppm	435 wppm
Q (l/h)	1089	1461	2466	2565	4185
Re_w	9573	11636	11952	9764	10805
$\dot{\gamma}_w$ (s^{-1})	226	263	218	184	275
τ_w (Pa)	0.225	0.285	0.396	0.422	0.933
$f(\times 10^{-3})$	8.00	5.75	2.75	2.73	2.27
DR%	0	23	63	65	70

It is very important to emphasize that the 175 and the 435 wppm solutions show similar results in the LDV experiments as will be shown in Section 4.2. This means that a limit for drag reduction is reached. A further increase of the polymer concentration does not alter the friction factor.

4.2. LDV EXPERIMENTS

In this section we will describe the results obtained from the LDV experiments. We focus our attention on the effect of the addition of polymers on the turbulence

Table III. Main flow parameters during the LDV experiments. Q: flow rate; Re, Re_w: Reynolds numbers based on bulk velocity U_b (and wall viscosity for the polymer solutions); Re_τ: Reynolds number based on friction velocity u_τ; U_c: centreline velocity; f: friction factor determined from pressure drop measurements; $\eta_w/\rho u_\tau$: viscous length scale.

solution	water	20 wppm	103 wppm	175 wppm	435 wppm
symbol	□	▽	■	○	▲
Q (l/h)	1089	1461	2466	2565	4185
Re, Re_w	9573	11636	11952	9764	10805
Re_τ	608	624	443	361	364
U_b (mm/s)	236	317	535	557	908
u_τ (mm/s)	15.0	17.0	19.9	20.6	30.6
U_c/u_τ	20.2	23.7	39.1	42.7	47.6
$f(\times 10^{-3})$	8.00	5.75	2.75	2.73	2.27
$\eta_w/\rho u_\tau$ (mm)	0.066	0.065	0.091	0.112	0.111

statistics for the three different concentrations (103, 175, 435 wppm). In Table II we present some data of these experiments.

The wall Reynolds number Re_w and the shear rate at the wall $\dot{\gamma}_w$ are determined following the procedure described in Section 2.1. All results are obtained at approximately $\mathrm{Re}_w \approx 10000$. The results of these experiments will be compared with LDV measurements for water and for a very dilute polymer solution of 20 wppm Superfloc A110 [7, 12]. We will display all velocity statistics in non-dimensional units (the so-called wall units). This means that velocities will be made non-dimensional with the friction velocity $u_\tau = \sqrt{\tau_w/\rho}$ and lengths with $\eta_w/(u_\tau \rho)$. The non-dimensional quantities will be denoted with a plus superscript.

An overview of the main characteristics of the experimental conditions is given in Table III.

4.2.1. *Mean Velocity*

In Figure 4 the non-dimensional mean velocity is plotted as function of the distance from the pipe wall (y^+ is the non-dimensional distance from the wall).

For water the mean velocity profile in the viscous sublayer and in the logarithmic region is given by respectively

$$U_x^+ = y^+, \quad y^+ < 5, \tag{13}$$

$$U_x^+ = 2.5 \ln(y^+) + 5.5, \quad y^+ > 30. \tag{14}$$

For drag-reducing fluids the same profile is found in the viscous sublayer. The logarithmic profile, however, shows an increase of the slope. For maximum drag reduction the relation is according to Virk [4]

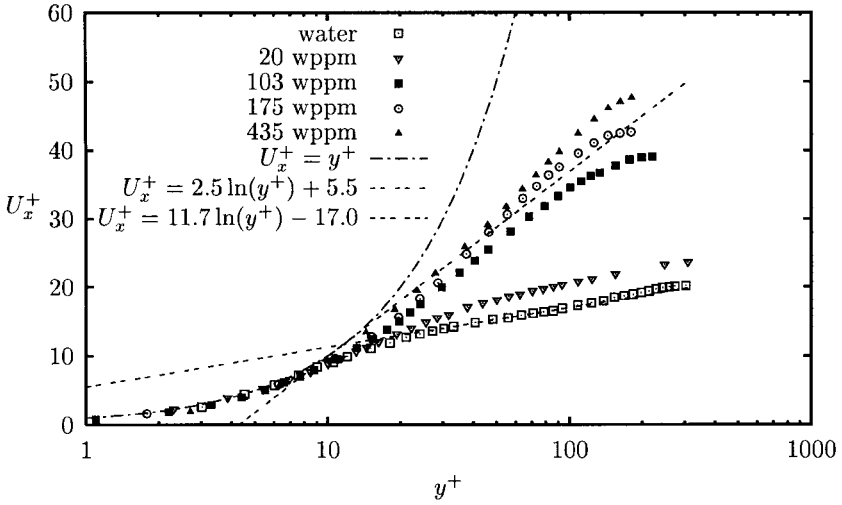

Figure 4. LDV measurements of the axial mean velocity in terms of wall units for water and for the polymer solutions. The lines are the profiles of Equations (13), (14) and (15). Flow conditions are given in Table III.

$$U_x^+ = 11.7\ln(y^+) - 17.0, \quad y^+ > 30. \tag{15}$$

For water the agreement between relations (13) and (14) and the experimental data is very good. The profile of the 20 wppm solution is shifted almost parallel upwards while the logarithmic region starts further away from the wall. For the more concentrated solutions there is a significant increase in the slope of the logarithmic profile. We see that the Virk asymptote is slightly exceeded for the 175 wppm and particularly for the 435 wppm solution. This effect is also noted by others [4, 14, 25].

4.2.2. *Turbulence Intensities*

In Figure 5 we present the root mean square of the axial velocity fluctuations: rms (u_x^+). For small concentrations the height of the peak increases with respect to water. However, when the concentration is increased further, the root mean square decreases to approximately the same value as for the solvent. Another effect as a function of the polymer concentration is a shift of the peak away from the wall (to higher wall units). Furthermore, Figure 5 shows that the root mean square of the axial velocity fluctuations is decreased near the wall, while the value is increased in the logarithmic layer. This corresponds with a larger gradient of the root mean square velocity fluctuations. An explanation for this is that the polymers produce a shear sheltering layer with high turbulence above it and low turbulence below it as described by Hunt and Durbin [26]. This is consistent with the numerical simulations of Sureshkumar et al. [8] and Dimitropoulos et al. [27], which show that the

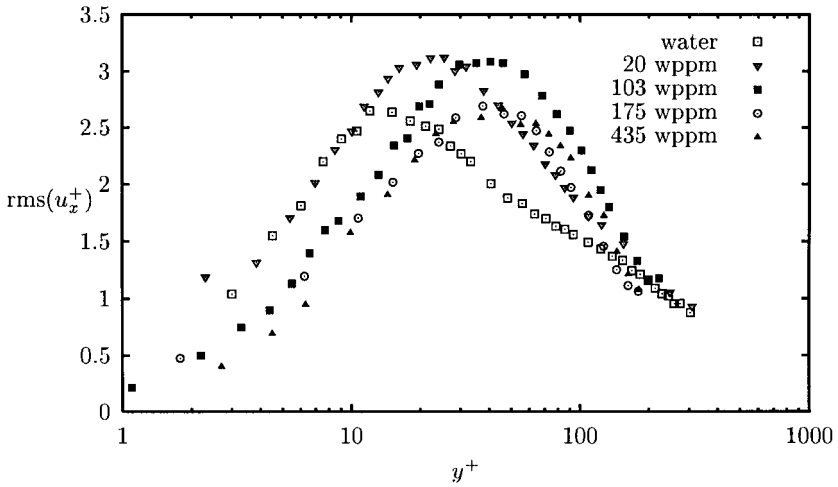

Figure 5. LDV measurements of the root mean square of the axial velocity for water and for the polymer solutions. Flow conditions are given in Table III.

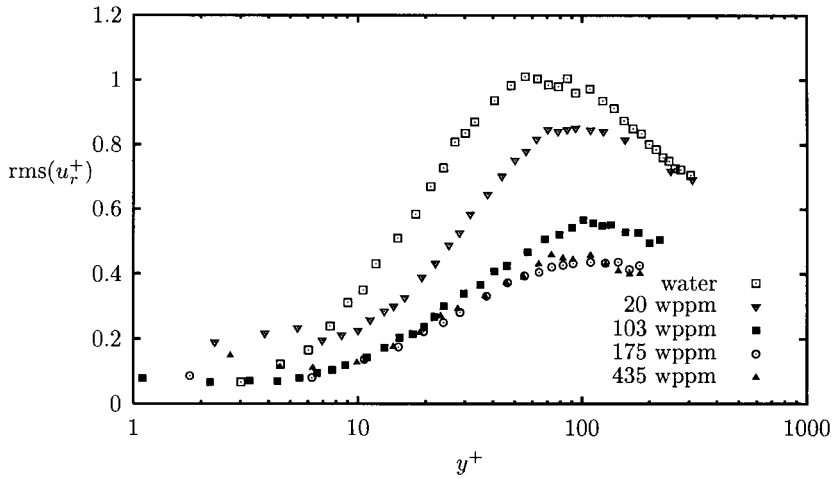

Figure 6. LDV measurements of the root mean square of the radial velocity for water and for the polymer solutions. Flow conditions are given in Table III.

maximum extension of the polymers occurs at approximately 20 wall units. In the centre of the pipe the results approach to a similar value for all concentrations.

The root mean square of the radial velocity fluctuations, rms (u_r^+), is plotted in Figure 6. These fluctuations are suppressed as a result of polymer addition for all locations in the pipe except in the viscous sublayer. The decrease is strongest for the high concentrations which show maximum drag reduction. The profile of the 20 wppm solution shows only a small decrease. The value of the root mean square of the radial velocity fluctuations approaches the value of water near the centre of the pipe while the strong drag-reducing solutions have a significantly

lower value. For all polymer solutions the location of the peak is shifted away from the wall though the shift for the radial velocity component is smaller than for the axial component. Similar effects for both the axial and radial root mean square are reported by Warholic et al. [15] and by direct numerical simulations [7, 8]. The main conclusion of the velocity fluctuation measurements is that drag reduction leads to modification of turbulent structures and energy particularly in the buffer layer.

4.2.3. *Turbulent, Solvent and Polymer Stress Contributions*

The mean shear stress in a fully developed pipe flow is a linear function of the radial coordinate between the zero value at the centreline and τ_w as given by Equation (1) at the wall. Furthermore, the mean shear stress $\mathcal{T}$ can be written as the sum of the Reynolds stress $\mathcal{T}_r$, the solvent (viscous) stress $\mathcal{T}_s$, and the polymeric stress $\mathcal{T}_p$. These terms also appear in Equation (10). Note that according to our notation the stress and all components of the stress are negative, because the pressure gradient in Equation (1) is negative. For reasons of simplicity we will display the stress contributions as positive quantities. For the dimensionless values of these stresses (non-dimensionalized with τ_w) then follows:

$$\mathcal{T}^+ = \frac{2r}{D}, \tag{16}$$

$$\mathcal{T}_r^+ = \frac{1}{u_\tau^2}\langle u_x' u_r' \rangle, \tag{17}$$

$$\mathcal{T}_s^+ = -\frac{1}{\rho u_\tau^2}\eta_s \frac{dU_x}{dr}, \tag{18}$$

$$\mathcal{T}_p^+ = \mathcal{T}^+ - \mathcal{T}_r^+ - \mathcal{T}_s^+. \tag{19}$$

The turbulent shear stress (Reynolds stress) is shown in Figure 7.

The addition of the polymers results in a strong decrease (up to 75%) of the Reynolds stress. This decrease becomes stronger when the concentration increases and at the two most concentrated solutions (175 and 435 wppm) a lower limit is reached. The decrease of the Reynolds stress for increasing polymer concentration is also reported in other experimental work such as Harder and Tiederman [9], Wei and Willmarth [10], and Den Toonder [12] and in the direct numerical simulation of Sureshkumar et al. [8]. However, the effects are weaker because lower polymer concentrations are used. In similar experimental conditions as used here, Warholic et al. [14, 15] have reported an almost zero Reynolds stress for surfactant and polymer solutions near maximum drag reduction. We note that in our experiments the Reynolds stresses at maximum drag reduction are significantly reduced but they remain definitely non-zero.

The correlation coefficient ρ of the axial and radial velocity components is illustrated in Figure 8. The correlation coefficient is defined by

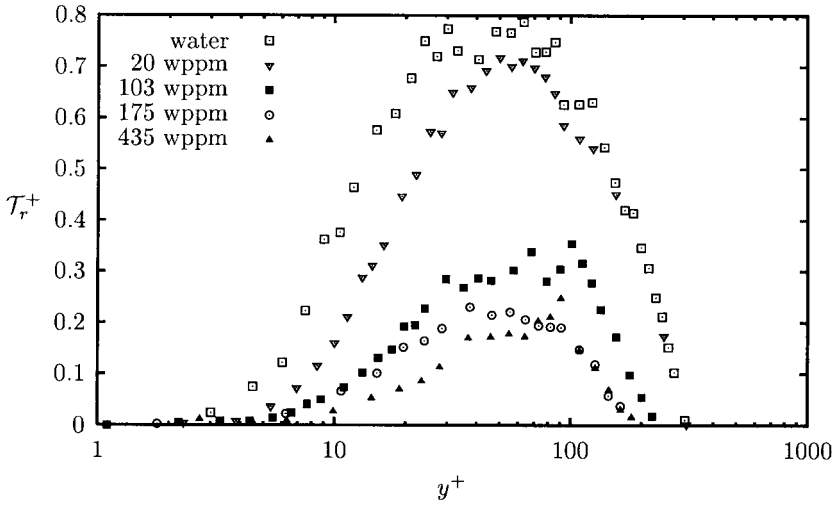

Figure 7. LDV measurements of the turbulent shear stress for water and for the polymer solutions. Flow conditions are given in Table III.

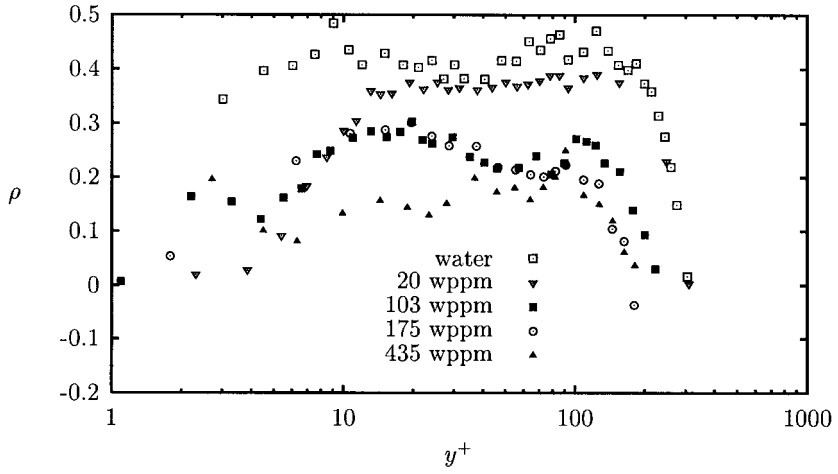

Figure 8. LDV measurements of the correlation coefficient of the axial and radial velocity components for water and for the polymer solutions. Flow conditions are given in Table III.

$$\rho = \frac{\langle u_x' u_r' \rangle}{\sqrt{\langle u_x'^2 \rangle}\sqrt{\langle u_r'^2 \rangle}}. \tag{20}$$

This quantity also decreases at all radial positions as a function of polymer concentration. The relative decrease is, however, less than for the turbulent stress.

Next we consider the various contributions to the mean shear stress $\mathcal{T}$. First we consider the case of water which is shown in Figure 9. In this figure we have plotted the measured Reynolds stress ($\mathcal{T}_r^+$, Equation (17)) as well as the solvent stress ($\mathcal{T}_s^+$, Equation (18)). The latter is computed from a derivative of the mean velocity

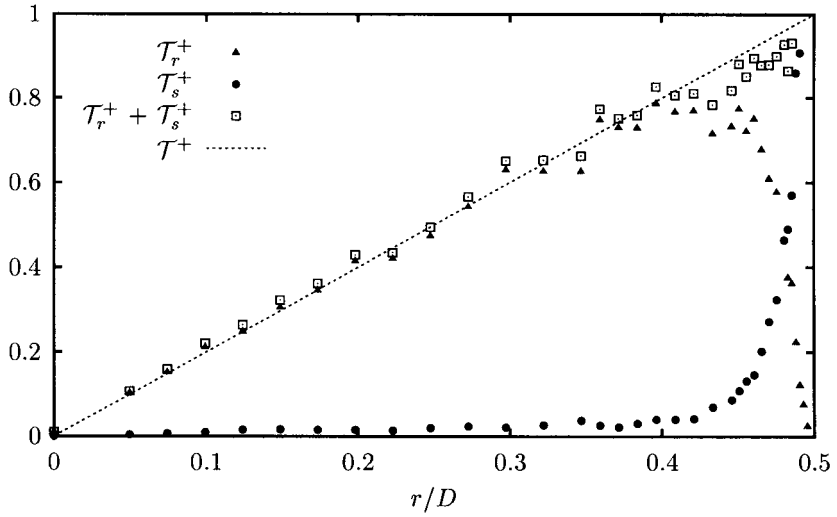

Figure 9. The various contributions to the mean shear stress for water as a function of the pipe radius. $\mathcal{T}_r^+$: Reynolds stress; $\mathcal{T}_s^+$: solvent stress; $\mathcal{T}^+$: (theoretical) mean shear stress. Re $\approx$ 9600.

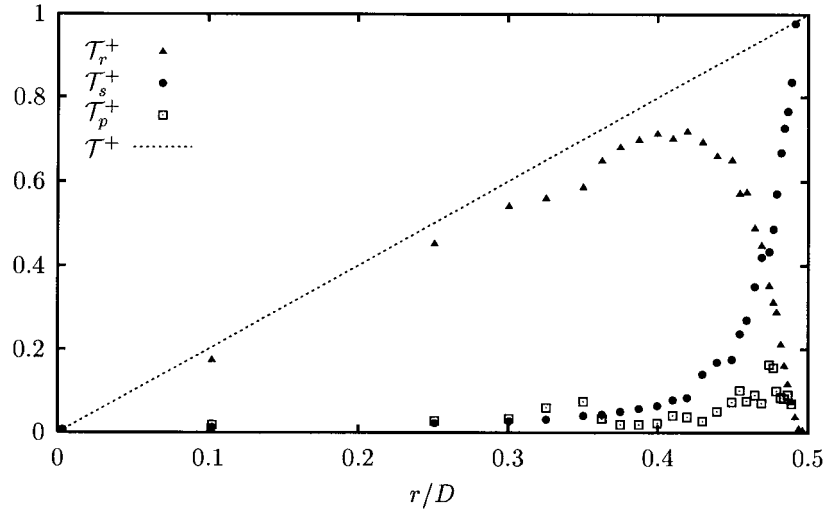

Figure 10. The various contributions to the shear stress as a function of the pipe radius for the 20 wppm solution [12]. $\mathcal{T}_r^+$: Reynolds stress; $\mathcal{T}_s^+$: solvent stress; $\mathcal{T}_p^+$: polymer stress; $\mathcal{T}^+$: (theoretical) mean shear stress. $\mathrm{Re}_w \approx 11600$.

profile which is determined by spline interpolation of the measurements. Note that the solvent stress is based on the viscosity of the solvent (water) only. Also the sum of these two contributions is shown and compared to the theoretical mean shear stress ($\mathcal{T}^+$, Equation (16)), which is linear across the pipe diameter. The

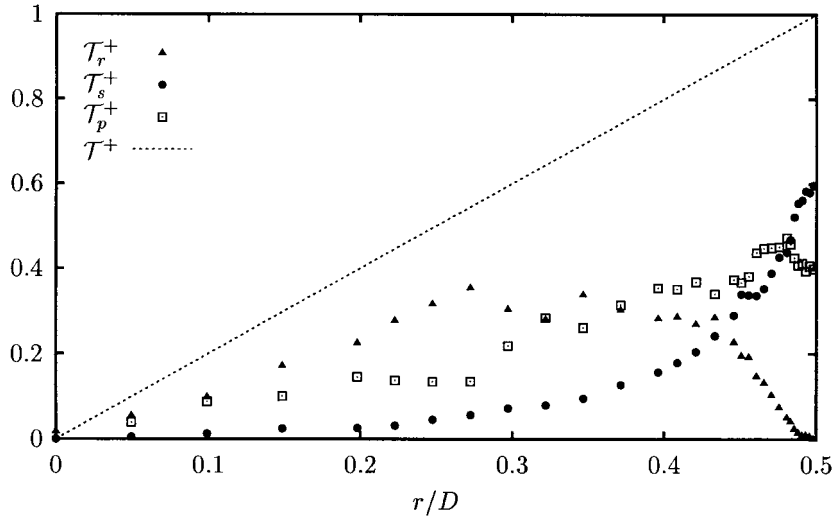

Figure 11. The various contributions to the shear stress as a function of the pipe radius for the 103 wppm solution. $\mathcal{T}_r^+$: Reynolds stress; $\mathcal{T}_s^+$: solvent stress; $\mathcal{T}_p^+$: polymer stress; $\mathcal{T}^+$: (theoretical) mean shear stress. $\mathrm{Re}_w \approx 12000$.

agreement is excellent except for the region near the wall which may be explained by inaccuracies in the interpolation procedures for steep velocity gradients.

The contributions by the Reynolds stress, the solvent stress and the polymeric stress for the three polymer solutions are plotted in Figures 10–13. The polymer stress has been obtained as the mean shear stress minus the sum of the turbulent and solvent stresses (Equation (19)). The fact that the sum of solvent and turbulent stresses no longer equals the mean stress is called the Reynolds stress deficit. We see that for the 20 wppm solution the polymer stress contribution is quite small and only non-negligible close to the wall. The more concentrated solutions show that the main contribution to the total stress comes from polymers taking over this role from turbulence. Especially the 435 wppm solution has a polymer stress contribution which is over 60% of the total stress. Furthermore, the polymer stress for the strong drag-reducing solutions is almost a linear function of the radial location. This means that the relative polymer stress contribution is approximately the same for each radial location.

4.3. THE MEAN AND TURBULENT ENERGY BUDGET

Let us now turn to the energy budgets of Equations (11) and (12) for our experimental data with water and with the 175 wppm polymer solution. We consider the area-integrated budget, which means that all terms in Equations (11) and (12) are integrated over the pipe cross section (denoted with 'S'). The integral of the transport (divergence) terms (T_u) then becomes zero. For the mean flow energy of Equation (11) this means that the production of mean flow energy due to the

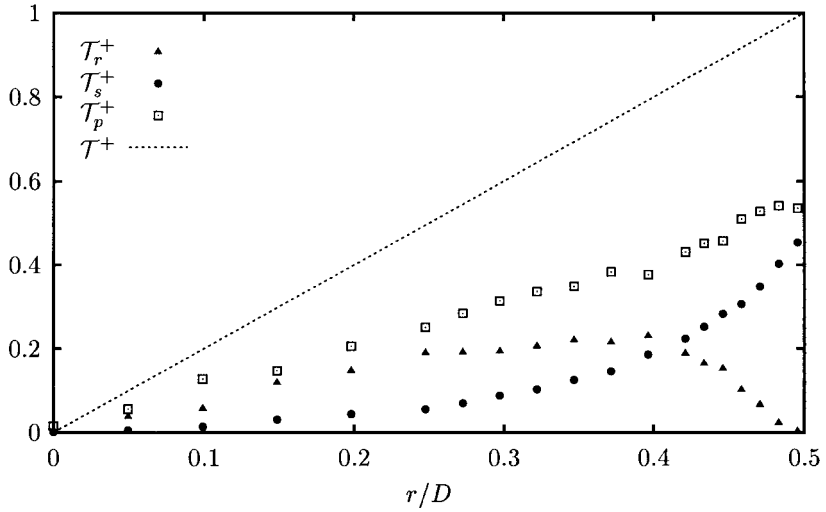

Figure 12. The various contributions to the shear stress as a function of the pipe radius for the 175 wppm solution. $\mathcal{T}_r^+$: Reynolds stress; $\mathcal{T}_s^+$: solvent stress; $\mathcal{T}_p^+$: polymer stress; $\mathcal{T}^+$: (theoretical) mean shear stress. $\mathrm{Re}_w \approx 9800$.

imposed pressure gradient ('gain') should be in balance with the deformation work, the viscous dissipation by the mean flow and the dissipation by mean polymeric stresses ('loss'):

$$\int_S P_u = \int_S -D_u + \int_S E_s + \int_S E_p. \tag{21}$$

For the kinetic energy of the turbulence there should be a balance between the production of turbulent energy on one side and the viscous dissipation and the polymeric stress work on the other side. Again the integral of the transport terms (T_k) is zero. Equation (12) then becomes

$$\int_S P_k = \int_S \epsilon_s + \int_S \epsilon_p. \tag{22}$$

The terms in Equation (21) are given in Table IV for water and for the 175 wppm polymer solution. For the case of water all terms have been measured independently by LDV. In other words, the terms on the right-hand side should add up to the terms on the left-hand side of Equation (21). We see that within an error of about 2% this is true and this is consistent with the stress profiles for water shown in Figure 9. It gives us confidence that our data are sufficiently accurate in order to estimate the contribution of the polymers to the kinetic energy budget by the difference between the measured terms. As additional information, the distribution of the terms in Equation (21) across the radial location is shown in Figure 14.

Let us next consider the results for the mean energy budget of the polymer solution which is given in the rightmost column of Table IV. The most important

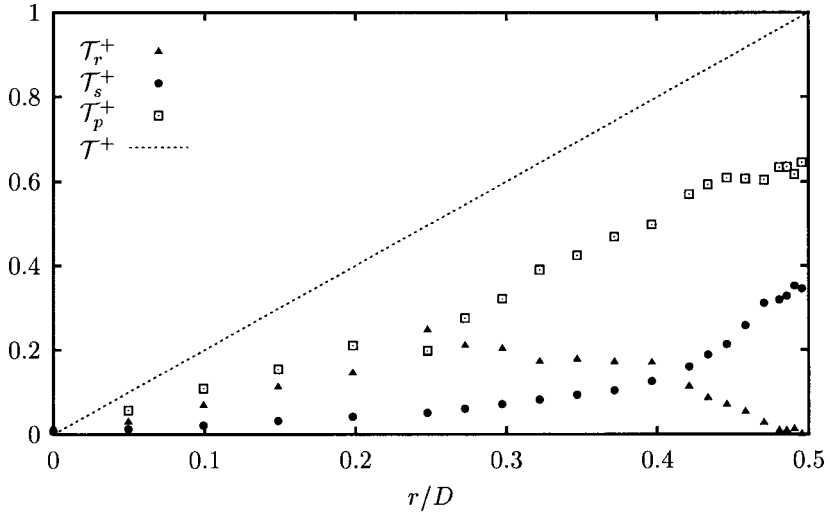

Figure 13. The various contributions to the shear stress as a function of the pipe radius for the 435 wppm solution. $\mathcal{T}_r^+$: Reynolds stress; $\mathcal{T}_s^+$: solvent stress; $\mathcal{T}_p^+$: polymer stress; $\mathcal{T}^+$: (theoretical) mean shear stress. $\mathrm{Re}_w \approx 10800$.

Table IV. The various mean flow energy budget terms for water and for the 175 wppm solution. All quantities are made non-dimensional with $\eta_w u_\tau^2$.

solution	water	175 wppm
$\int_S P_u$	2.94×10^4	3.08×10^4
$\int_S -D_u$	1.16×10^4	0.480×10^4
$\int_S E_s$	1.85×10^4	0.959×10^4
$\int_S E_p$	0	1.63×10^4
$\int_S(-D_u + E_s + E_p)$	3.01×10^4	3.07×10^4

result here is that the E_p term is the largest loss term on the right-hand side of the budget. This implies that most of the energy is transferred directly to the polymers and not by the route of turbulence. This is shown also in more detail in Figure 15 where the various budget terms are plotted.

We now turn to the budget of the turbulent kinetic energy. In this budget only the production P_k can be measured directly. In the integrated budget of Equation (22) for water the only remaining term is the viscous dissipation ϵ_s which should thus be equal to P_k. Alternatively, we can approximate ϵ_s by (see [28])

$$\epsilon_s \approx c_D \rho \frac{e^{3/2}}{D}, \tag{23}$$

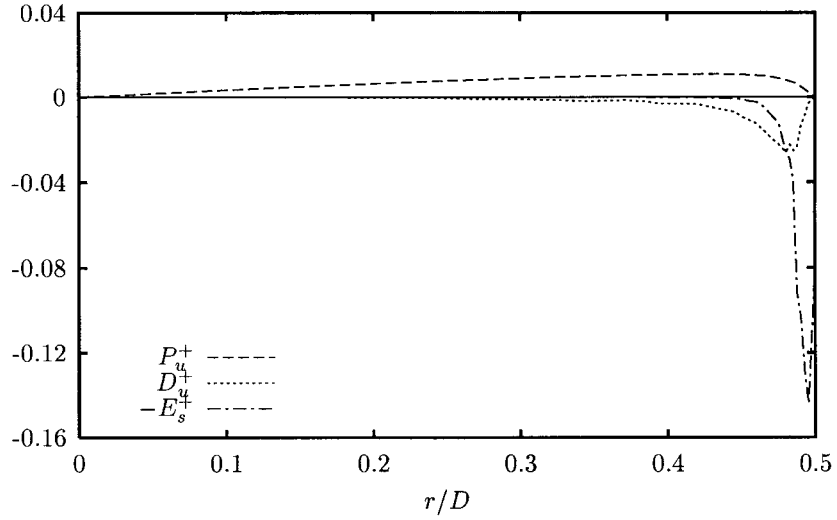

Figure 14. The various mean flow energy budget terms for water. Re $\approx$ 9600.

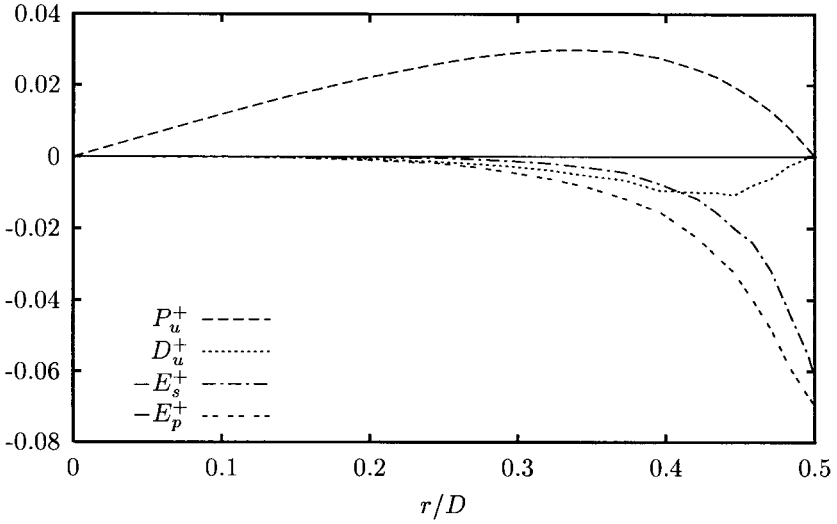

Figure 15. The various mean flow energy budget terms for the 175 wppm solution. $\mathrm{Re}_w \approx 9800$.

where c_D is a dimensionless constant and $e = (1/2)\langle u_i'^2 \rangle$ is the turbulent kinetic energy per unit mass. Since we cannot measure $\langle u_\theta'^2 \rangle$, we will only make an estimation by discussing the order of magnitude. Direct numerical simulations [7, 8] show that $\langle u_\theta'^2 \rangle$ is of the same order as $\langle u_r'^2 \rangle$ for both non-drag-reducing and drag-reducing flow. Therefore we will approximate the turbulent kinetic energy by $e = (1/2)(\langle u_x'^2 \rangle + 2\langle u_r'^2 \rangle)$. This estimation gives for our Newtonian flow a value of $c_D = 7.21$.

Table V. The various turbulent kinetic energy budget terms for water and for the 175 wppm solution. All quantities are made non-dimensional with $\eta_w u_\tau^2$.

solution	water	175 wppm
$\int_S P_k$	1.16×10^4	0.480×10^4
$\int_S \epsilon_s$	1.16×10^4	0.808×10^4
$\int_S \epsilon_p$	0	-0.328×10^4

The value of the constant c_D depends on the pipe geometry, e.g. through the Reynolds number, and on the dynamics of turbulence by which energy is transferred through a cascade process to dissipate into heat at the microscales. Let us now assume that the constant remains the same for the turbulent flow of the polymer solution. This allows us to compute ϵ_s for the polymer solution and the polymeric stress work ϵ_p from the difference with P_k. The results are given in Table V.

We find that the polymeric stress work ϵ_p becomes negative. In other words, the fluctuating polymeric stresses produce rather than dissipate kinetic energy. However, we must stress that this result depends strongly on our assumption that the constant c_D remains the same which requires an independent verification. Therefore we must conclude that although energy production by fluctuating polymer stresses can not be excluded, there is certainly no conclusive evidence for this. The process that energy is produced by fluctuating polymer stresses has also been suggested by Warholic et al. [14, 15], though the difference is that in their experiments the production of kinetic energy P_k is zero and thus the viscous dissipation ϵ_s is the opposite of the polymeric stress work ϵ_p.

5. Conclusions and Discussion

We have performed LDV measurements in a turbulent pipe flow with polymer additives. The polymer used is Superfloc A110, which is partially hydrolyzed polyacrylamide. The conditions of the flow are at maximum drag reduction near the Virk asymptote [4]. It is important to notice that in all cases that we have observed, the flow is turbulent.

The amount of drag reduction is measured in terms of the change in the Fanning friction factor as a function the (wall) Reynolds number. The use of a wall Reynolds number follows from the fact that for non-Newtonian fluids, like the shear thinning polymer solutions used in our case, the viscosity does not have a constant value. Therefore we cannot just use the conventional Reynolds number definition which is based on a constant viscosity everywhere in the flow. The wall Reynolds number is based on an introduction of a wall viscosity η_w which is related to the wall shear

stress. The latter has a linear relation with the measured pressure drop over a pipe segment. We think this is a appropriate definition as has been found earlier in the literature [2, 17, 18].

All our LDV experiments with polymer solutions are performed at $\mathrm{Re}_w \approx 10000$ and show a high rate of drag reduction. The difference in the measured velocity statistics between the two highest concentrations is very small, becoming independent of the concentration, so that we can state that the asymptotic value for drag reduction is reached. The results of these measurements are compared with our measurements with water and with measurements with a less concentrated polymer solutions [7, 12]. Most effects are much stronger for the strongly drag-reducing solutions compared to the results of Den Toonder.

The main results of the profile measurements are the following: as a result of the addition of polymers the flow rate strongly increases, which is consistent with drag reduction at constant pressure drop. In the wall region the buffer layer thickens and the velocity profile in the logarithmic region has a larger slope. Our profiles of the mean velocity in the logarithmic region are consistent with Equation (15).

The peak of the root mean square of the axial velocity fluctuations is increased for small polymer concentrations and shifts away from the wall. However, for the highest concentrations the height of the peak returns to the value found for water. So a maximum value is reached at some intermediate concentration. The root mean square of the radial velocity fluctuations shows a strong decrease and a small shift of the peak towards the centre of the pipe. The turbulent kinetic energy shows a shift from the normal (radial) to the streamwise (axial) component.

The Reynolds stress is strongly decreased at high polymer concentrations, but remains definitely non-zero. This is in contrast with the observations of Warholic et al. [14, 15] who found a Reynolds stress very close to zero for surfactant and polymer solutions. The sum of the solvent and Reynolds stress no longer equals the total stress, mainly due to the strongly decreased Reynolds stress. This is called the Reynolds stress deficit and the effect is more dominant for strong drag reducing solutions. This means that the polymers contribute significantly to the total stress, taking over this role from the turbulence.

Summarizing we find similar results as Warholic et al. [15] for the mean velocity and for the turbulence intensities, but the difference is a non-zero Reynolds stress in our case.

In the comparison of various terms in the mean energy budget we have found that most of the mean flow kinetic energy is transferred directly to the polymers and not to the turbulence. This corresponds with a direct suppression of the turbulent kinetic energy. Depending on the assumption made for the viscous dissipation we have found that the polymeric stress work can be negative. This latter behaviour is equivalent to a production of turbulence by the fluctuating polymer stresses.

References

1. Toms, B.A., Some observations on the flow of linear polymer solutions through straight tubes at large Reynolds numbers. In: *Proceedings 1st International Congress on Rheology*. North Holland, Amsterdam (1949) pp. 135–141.
2. Gyr, A. and Bewersdorff, H.-W., *Drag Reduction of Turbulent Flows by Additives*. Kluwer Academic Publishers, Dordrecht (1995).
3. Lumley, J.L., Drag reduction by additives. *Ann. Rev. Fluid Mech.* **1** (1969) 367–384.
4. Virk, P.S., Drag reduction fundamentals. *AIChE J.* **21** (1975) 625–656.
5. Lumley, J.L., Drag reduction in turbulent flow by polymer additives. *J. Polymer Sci.* **7** (1973) 263–290.
6. Tiederman, W.G., The effect of dilute polymer solutions on viscous drag and turbulent structure. In: Gyr, A. (ed.), *IUTAM Symposium: Structure of Turbulence and Drag Reduction*. Springer-Verlag, New York (1989) pp. 187–200.
7. Den Toonder, J.M.J., Hulsen, M.A., Kuiken, G.D.C. Nieuwstadt, F.T.M., Drag reduction by polymer additives in a turbulent pipe flow: Laboratory and numerical experiments. *J. Fluid Mech.* **337** (1997) 193–231.
8. Sureshkumar, R., Beris, A.N. and Handler, R.A., Direct numerical simulation of the turbulent channel flow of a polymer solution. *Phys. Fluids* **9** (1997) 743–755.
9. Harder, K.J. and Tiederman, W.G., Drag reduction and turbulent structure in two-dimensional channel flows. *Philos. Trans. Roy. Soc. London A* **336** (1991) 19–34.
10. Wei,T. and Willmarth, W.W., Modifying turbulent structure with drag-reducing polymer additives in turbulent channel flows. *J. Non-Newtonian Fluid Mech.* **245** (1992) 619–641.
11. Willmarth, W.W., Wei, T. and Lee, C.O., Laser anemometer measurements of Reynolds stress in a turbulent channel flow with drag reducing polymer additives. *Phys. Fluids* **30** (1987) 933–935.
12. Den Toonder, J.M.J., Drag reduction by polymer additives in a turbulent pipe flow: Laboratory and numerical experiments. Ph.D. Thesis, Delft University of Technology, Delft, The Netherlands (1995).
13. Gampert, B. and Yong, C.K., The influence of polymer additives on the coherent structure of turbulent channel flow. In: Gyr, A. (ed.), *IUTAM Symposium: Structure of Turbulence and Drag Reduction*. Springer-Verlag, New York (1989) pp. 223–232.
14. Warholic, M.D., Schmidt, G.M. and Hanratty, T.J., The influence of a drag-reducing surfactant on a turbulent velocity field. *J. Fluid Mech.* **388** (1999) 1–20.
15. Warholic, M.D., Massah, H. and Hanratty, T.J., Influence of drag-reducing polymers on a turbulence: effects of Reynolds number, concentration and mixing. *Exp. Fluids* **27** (1999) 461–472.
16. Schlichting, H., *Boundary Layer Theory*, 6th edn. McGraw-Hill, New York (1987).
17. Pinho, F.T. and Whitelaw, J.H., Flow of non-Newtonian fluids in a pipe. *J. Non-Newtonian Fluid Mech.* **34** (1990) 129–144.
18. Draad, A.A., Kuiken, G.D.C. and Nieuwstadt, F.T.M., Laminar-turbulent transition in pipe flow for Newtonian and non-Newtonian fluids. *J. Fluid Mech.* **377** (1998) 267–312.
19. Bird, R.B., Armstrong, R.C. and Hassager, O., *Dynamics of Polymer Liquids*, Vol. 1, 2nd edn. John Wiley, New York (1987).
20. Batchelor, G.K., *An Introduction to Fluid Dynamics*. Cambridge University Press, Cambridge (1967).
21. Draad, A.A., Laminar-turbulent transition in pipe flow for Newtonian and non-Newtonian fluids. Ph.D. Thesis, Delft University of Technology, Delft, The Netherlands (1996).
22. Den Toonder, J.M.J., Draad, A.A., Kuiken, G.D.C. and Nieuwstadt, F.T.M., Degradation effects of dilute polymer solutions on turbulent drag reduction in pipe flows. *Appl. Sci. Res.* **55** (1995) 63–82.

23. Inerthal, W. and Wilski, H., Drag reduction experiments with very large pipes. *Coll. & Polymer Sci.* **263** (1985) 217–229.
24. Kenis, P.R., Turbulent flow friction reduction effectiveness and hydrodynamic degradation of polysaccharides and synthetic polymers. *J. Appl. Polymer Sci.* **15** (1971) 607–618.
25. Virk, P.S., Mickley, H.S. and Smith, K.A., The ultimate asymptote and mean flow structure in Toms' Phenomenon. *ASME, J. Appl. Mech.* **37** (1970) 480–493.
26. Hunt, J.C.R. and Durbin, P.A., Perturbed vortical layers and shear sheltering. *Fluid Dynam. Res.* **24** (1999) 375–404.
27. Dimitropoulos, C.D., Sureshkumar, R. and Beris, A.N., Direct numerical simulation of viscoelastic turbulent channel flow exhibiting drag reduction: Effect of variation of rheological parameters. *J. Non-Newtonian Fluid Mech.* **79** (1998) 433–468.
28. Tennekes, H. and Lumley, J.L., *A First Course in Turbulence*. MIT Press, Cambridge, MA (1973).